Proceedings of 20th International Congress on Acoustics, ICA 2010

23-27 August 2010, Sydney, Australia

Multistatic detection and tracking using maximal length sequences

W. Jobst (1), D. Smith (2) and L. Whited (1)

(1) Applied Marine Physics, LLC, 1544 Marina Drive, Slidell, LA 70458 USA amp_jobst@bellsouth.net
(2) CyberSmiths, Inc., 3231 SW 105 Ct, Miami, FL 33165, USA david@cybersmiths.biz

PACS: .30.VH, 43.30.ZK, 43.60.GK, 43.60.JN

ABSTRACT

A simulation using maximal length sequences demonstrated the potential for detecting and tracking multiple near-surface targets in shallow, near-shore areas. In our simulation a low power, omnidirectional source and four omnidirectional hydrophones were arbitrarily located in water approximately 4 m deep. Using "channel digit response" processing and "block zeroing", the direct arrival, multipaths, clutter and reverberation were rejected, thereby transforming reverberation limited detection conditions into noise limited detection conditions. With the improved signal-to-interference ratio, a simple probability based algorithm demonstrated tracking of -20 dB targets at source-target distances of 250 m, the maximum range investigated.

I. BACKGROUND

Since their initial use in acoustic propagation studies more than fifty years ago, oceanographers and acousticians have used maximal length sequences (m-sequences) to investigate large scale ocean processes and long range sound propagation. Referenced papers describe early research and summarize more recent selected experiments [1-6]. In this paper we depart from previous work and through simulation, investigate the use of m-sequences for detecting and tracking multiple moving targets in an environment with noise, multipath propagation, surface reverberation, bottom reverberation and clutter. Unlike our previous work [7], the simulated transmitted m-sequence is bandpass filtered, and each scattering source is modelled as an infinite impulse response linear filter. The transmitter is a single omnidirectional projector and the multistatic receivers are four individual omnidirectional hydrophones. The source and receivers are at different water depths, all less than 4 m.

Our m-sequence signal processing follows a "channel digit response" design first described by T. Birdsall and K. Metzger [8], but applied under their guidance in earlier research [9, 10]. Our algorithm for removing interference follows a "zeroing" approach described by H. Chang in a Doctoral dissertation under T. Birdsall [11] and applied in more recent work by H. DeFerrari and A. Rogers [12]. Our block zeroing and m-sequence ellipse tracking algorithms build on work previously introduced by the authors [7].

II. BACKGROUND

While the following material is available in the referenced papers, it is summarized here for clarity and to briefly describe our ocean acoustic channel simulation.

Our transmitted bandpass signal is a phase-modulated 25 KHz carrier in which the phase modulation is derived from the mathematical m-sequence. Specifically, our simulated transmitted bandpass signal is

$$s(t) = A\cos\left(2\pi f_0 + b(t)\phi\right), \tag{1}$$

where the modulation sequence, $b(t)$ = {+1,-1,-1,-1,,+1,…}, is obtained from an m-sequence of length L = 1023 digits. The carrier frequency, f_0, is 25 KHz, and the phase angle is chosen to be the period matched phase angle, reference [8], $\phi = \tan^{-1}\left(\sqrt{L}\right)$. A is a constant amplitude determined from the simulated 174dB projector source level, and we have chosen 24 carrier cycles per digit. A segment of the transmitted m-sequence is shown in Figure 1 after filtering with a 2000 Hz finite impulse response filter.

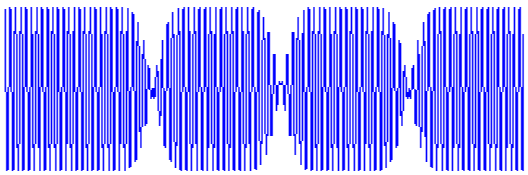

Figure 1: Segment of the filtered bandpass m-sequence

We model the ocean acoustic channel as a linear system in which the received signal, $r(t)$, is the convolution of the channel impulse response, $h(t)$, and the transmitted signal, $s(t)$

$$r(t) = \int h(t-\alpha)\cdot s(\alpha)d\alpha. \tag{2}$$

If we choose the transmitted signal to be the convolution of a pulse, *p(t)*, and a modulating m-sequence, we can use the properties of the m-sequence to obtain the response of the ocean acoustic channel to a transmitted pulse. Transforming to the frequency domain, we obtain

$$R(\omega) = H(\omega) \cdot P(\omega) \cdot M(\omega). \quad (3)$$

Since $M(\omega) \cdot M(\omega)^*$ is a constant, we may divide both sides of equation (3) by $M(\omega)$ and then multiply numerator and denominator of the left-hand side by the complex conjugate. (The "divide by zero" problem is avoided by choosing m-sequence modulation.) Transforming back to the time domain, we obtain the ocean response to a transmitted pulse by simply correlating the received signal with the m-sequence conjugate.

$$\int h(t-\alpha)\, p(\alpha) d\alpha = \int r(\alpha) \cdot m^*(t+\alpha) \cdot d\alpha \quad (4)$$

We will refer to the transformed received waveform (right hand side of equation (4)) as being in the "Channel Digit Response" (CDR) domain to distinguish the waveform from the time domain.

III. ACOUSTIC CHANNEL SIMULATION

Just as equation (4) places no restriction, other than linearity, on the transmitted pulse, *p*(*t*), no restriction is placed on the ocean acoustic channel impulse response, *h*(*t*). The left-hand side of equation (4) was modelled by convolving the filtered, transmitted pulse with more than 5000 point reflectors, each reflector delayed and appropriately scaled to represent the direct arrival, multipaths, clutter, surface reverberation, bottom reverberation and a moving target. To include the possibility that each scatterering source may behave as a linear filter, each point reflector was convolved with an infinite impulse response filter.

The ocean channel was assumed to be isovelocity, although a more complete model may be warranted in practice. An accurate representation of the ocean bottom generally requires measurements that are site specific. Consequently, we chose to make the ocean bottom infinitely attenuating, although again, a more complete model may be warranted. Surface reflected paths are included, both on the source-target path and on the target-hydrophone path. Bandlimited ambient noise representative of shallow water has been added to the simulation. Received signals are generated independently for each hydrophone.

At each hydrophone, the received signal, *r*(*t*), is demodulated and correlated with the m-sequence conjugate, following equation (4), to form the channel digit response. A representative example of the CDR domain response magnitude is shown in Figure 2.

In Figure 2 ambient noise is shown in segments labelled "A", both at the beginning of the sequence prior to the direct path arrival and at the end of the sequence after reverberation energy has decreased below ambient noise. The direct arrival and 19 clutter arrivals occur near "B". A continuum of bottom and surface scattering dominates region "C" until an arbitrary physical boundary is reached at "D". At "D" reverberation begins to decrease until it is below ambient noise. The ordinate is in units of energy on a decibel scale and includes demodulation and CDR processing gains. The red CDR domain data segment has been selected for block zeroing in later processing.

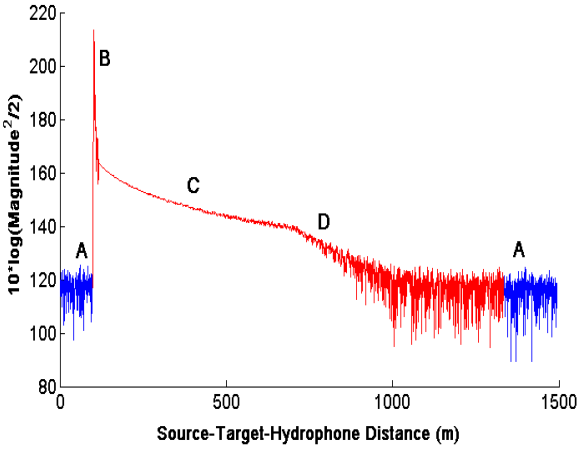

Figure 2: Channel digit response magnitude at hydrophone 1.

IV. BLOCK ZEROING

Block zeroing is the process of setting segments of interference in the CDR domain to zero, and then transforming from the CDR domain back to the time domain. The result of these operations is a new time domain signal with interference removed. These somewhat counter-intuitive operations are possible because of two m-sequence properties. The first of these properties, the correlation property, is that the right-hand side of equation 4 maps *L* time domain m-sequence complex samples onto a single CDR domain complex sample.

The significance of this mapping was probably not fully recognized until the research by Birdsall, Metzger and Chang. They recognized that *all time domain energy related to a CDR domain sample could be removed by simply setting the CDR domain sample to zero and then inverse transforming back to the time domain!* We have extended this concept from zeroing a few unwanted arrivals to block zeroing large segments of unwanted interference. In Figure 2 the direct arrival, clutter and the reverberation continuum shown in red were block zeroed, and the resulting signal was transformed back to the time domain prior to target detection and tracking.

If block zeroing segments of CDR domain data is somewhat counter-intuitive, then block zeroing data segments containing the target is even more so. The second, and often overlooked "uniform sidelobe energy distribution" property, is due to the pseudo-randomness of m-sequences. The sidelobe energy distribution property can best be understood by examining Doppler-shifted replicas of the received signal, each processed to determine a channel digit response. Because of its similarity to the ambiguity function first proposed by Woodward [13], we also refer to this as an "ambiguity function".

In Figure 3 the ambiguity function for a -20 dB moving target with multipaths is shown. To illustrate the uniform distribution of energy in the sidelobes of the target signal, ambient noise, the direct arrival, clutter and reverberation are not included in the figure. At each Doppler, a frequency shifted and time corrected replica of the received signal has been correlated with the m-sequence, following equation 4. (Also see reference [7].) Only the first 600 m of the 1500 m sequence is shown

Because the m-sequence is pseudorandom, correlating an unshifted m-sequence with a Doppler-shifted m-sequence is similar to correlating noise with Doppler-shifted noise. Consequently, the correlation operation distributes sidelobe energy uniformly with range. Specifically, the zero Doppler "slice" along the range axis is more than 20 dB below the target energy peak with similar energy at all ranges. Because of this property, zeroing a segment of the zero Doppler correlation, e. g. the red segment of Figure 2, *removes target energy approximately in proportion to the fraction of total samples zeroed*. The remaining m-sequence segments remain correlated, although separated in CDR range. The resulting coherent signal gain is therefore $20 \cdot \log(L-Q)$, where Q is the number of CDR domain samples zeroed. Despite the loss of signal gain, block zeroing has transformed an extremely difficult reverberation-limited detection problem into a tractable noise-limited detection problem.

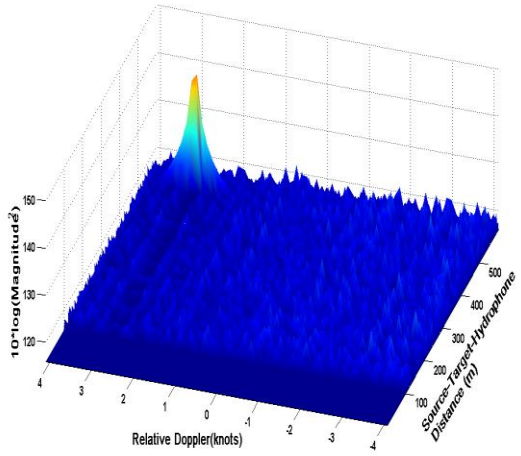

Figure 3: Ambiguity function for a -20 dB moving target. Sidelobe energy is approximately uniform with range.

V. TRACKING WITH M-SEQUENCES

For multistatic systems with omnidirectional receivers and an omnidirectional sound source, a detection on a source-receiver pair determines the time for energy to propagate from the source to the target and then to the receiver. When converted into distance, the locus of points with constant distance is an ellipse with foci at the source and hydrophone. Detections on two receivers determine two ellipses with up to four intersections, so a target cannot be uniquely located with two receivers unless some solutions can be eliminated, perhaps due to harbor boundaries. Detections on three receivers can uniquely determine target location. However, the ellipses may not intersect at a point. (See reference [7].) In Figure 4 we show the ellipses generated by simultaneous detections of a -20 dB target at coordinates (70,250) at four hydrophones.

Because of errors in estimating sound speed and errors in determining hydrophone locations, it is unlikely that three or more ellipses generated from detections at multiple hydrophones will intersect at a point. We have used a spatial filter that considers the variance due to hydrophone positioning, source positioning and water temperature. The color bar indicates the number of hydrophones that are holding the target at each 1m x 1m range cell after spatial filtering. For example, two ellipses passing through a single cell and one ellipse passing through an adjacent cell would generate a "cell count" slightly less than 3. Cells colored blue indicate that only a single source-receiver pair has a target ellipse passing through that cell. The red color at the intersection of four ellipses indicates that all four hydrophones are holding the target at approximately the same coordinates. The location of targets is determined by maxima in ellipse intersection constructions similar to Figure 4.

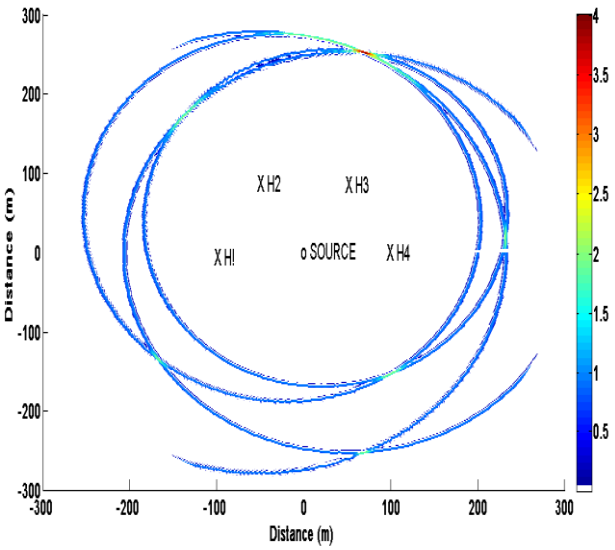

Figure 4: Ellipses generated by detections at four hydrophones. The color bar indicates the number of hydrophones that have detected a target in each 1m x 1m cell after spatial filtering. Ellipse segments more than 300 m from the source are not shown.

Ellipses generated by successive m-sequence detections can generate a target track. In Figure 5, a -20 dB target started at coordinates (70,250) and travelled at 1.5 kn at 1.5 m depth. Simulated Lloyd's mirror [14] surface reflected paths were included in both source-target propagation and target-hydrophone propagation. To counter destructive interference from surface-reflected paths and to minimize false alarms due to noise, we required 3 out of 6 successive envelope amplitude samples to exceed a threshold 10 dB above mean ambient noise. To further reduce false alarms due to noise, we required that the target be detected on at least three hydrophones and that target detection ellipses be sufficiently close to exceed a nominal "2.7 hydrophones" on our spatial filter scale previously described. The missing track point is the result of Lloyd's mirror surface interference and consequent failure to meet the 3 out of 6 successive envelope amplitude detections criteria on at least 3 hydrophones.

As an aid to target classification, target strength is shown on the color bar in Figures 5, 6 and 7. Target strength is estimated from the maximum received signal at detecting hydrophones, and then converted to target strength through a transmission loss model. In our simulation spherical spreading was assumed corresponding to isovelocity propagation conditions.

In Figure 6 two -20 dB targets are simulated, both at 1.5 m depth. The target with a closest point of approach of 250 m exceeds the 300 m maximum displayed source-target distance at the beginning and end of its track, so only the center segment of the track is shown. The track for the target proceeding toward the source is identical to that presented in Figure 5 when only a single target was present. Our experi-

ence has been that multiple target tracking is most effective when targets have similar acoustic target strength.

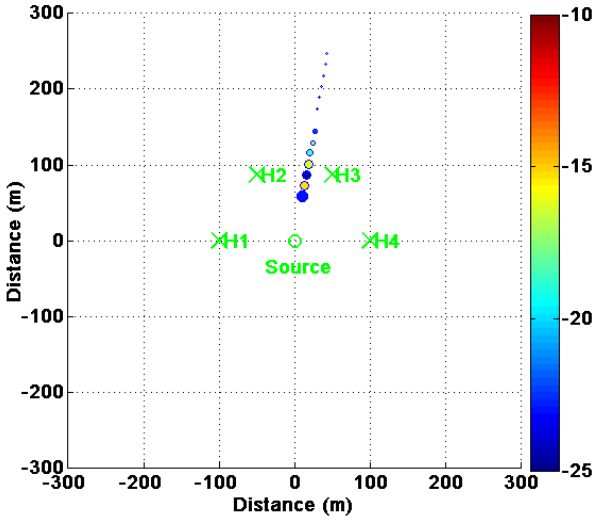

Figure 5: -20 dB target track segment. The target is at 1.5 m depth. The largest points are most recent. Color indicates target strength estimated from energy received at tracking hydrophones. Approximately 200 m of track is shown.

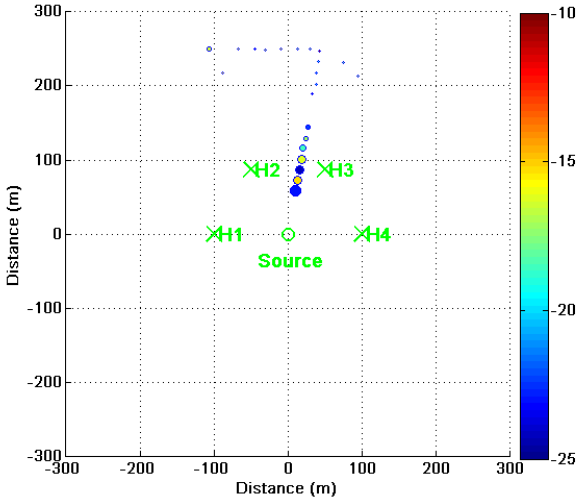

Figure 6: Two -20 dB target track segments. Both targets are at 1.5 m depth. Segments of the most distant track (250 m closest point of approach to the source) exceed the maximum displayed source-target-receiver distance and are not shown.

Unfortunately, m-sequences no longer have well-behaved sidelobe properties after sequence segments are removed through block zeroing. Unlike Figure 3 where sidelobes are more than -20 dB below the pulse peak amplitude, sidelobe structure after zeroing depends upon the CDR domain segment that has been zeroed. To avoid spurious detections on the sidelobes of high energy targets, we require less energetic targets to be no more than 10 dB below the energy of the principal return. This approach has been applied to Figure 7 where a -10 dB target is proceeding with a closest point of approach of 250 m while a -20 dB target is proceeding toward the source as before. The smaller target is initially detected and tracked much closer to the source than in previous cases.

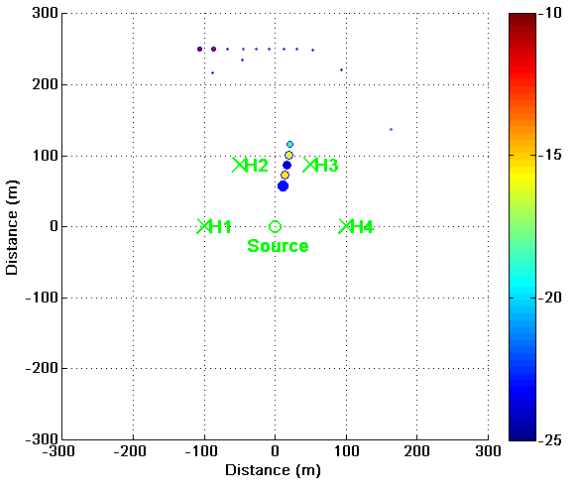

Figure 7: Two target track segments. A -10 dB target is at 250 m closest point of approach and 4 m depth. A -20 dB target is proceeding as in Figures 5 and 6.

We have only recently begun our investigation of multiple target tracking, and our findings are preliminary. In general, the high signal-to-interference ratios generated by CDR processing and block zeroing appear to make automated detection and tracking of single targets feasible. As the number of targets increases, the number of ellipses also increases, and the likelihood of generating false track points due to spurious ellipse intersection becomes a concern. Also ambiguity function sidelobes from large targets can make detection of less energetic targets more difficult. A more complex tracking algorithm, possibly a recursive implementation of equation (4), could address these issues

VI. CONCLUSIONS

There are many unknowns and technical challenges between a successful simulation and an in-water demonstration. Equipment dynamic range, multi-static acoustic target strength, non-linear scattering and near-shore currents are a few of the issues that might place additional constraints on the use of m-sequences. Setting these issues aside for future research, we have shown, using a simulation based on linear system modelling, that the direct arrival, multipaths, clutter and a continuum of reverberation can be removed through block zeroing. We have demonstrated that it may be possible to transform a clutter and reverberation limited detection problem into a much simpler noise limited detection problem. The high signal-to-noise ratios generated by interference removal allow multistatic detection and tracking with a simple ellipse intersection algorithm. A shallow water, multistatic detection and tracking system may therefore be feasible.

The authors gratefully acknowledge helpful discussions with T. Birdsall and Kurt Metzger (University of Michigan, Ann Arbor), and H. DeFerrari (University of Miami). These discussions have spanned more than 40 years. The authors also gratefully acknowledge helpful engineering and technical discussions with David Small (Naval Oceanographic Office).

REFERENCES

1. T. G. Birdsall, "MIMI multipath measurements", *J. Acoust. Soc. Am.* **38**, p. 919, (1965)
2. M. Kronengold and J. Lowenstein, "System for the study of underwater acoustic propagation" *J. Acoust. Soc. Am.* **38,** p. 918 (1965)
3. J. Steinberg and T. Birdsall, "Underwater sound propagation in the Straits of Florida" *J. Acoust. Soc. Am.* **39**, pp. 301-315 (1966)
4. K. Metzger Jr., *Signal Processing Equipment and Techniques for Use in Measuring Acoustic Multipath Struc tures* (Ph.D. Dissertation, University of Michigan Disser tation Services, 1983) 305 pp.
5. W. Munk, A. Baggeroer et al., "The Heard Island papers" (A collection of 17 papers) *J. Acoust. Soc. Am.* **96**, pp. 2327-2484 (1994)
6.. J. Colosi, A. Baggeroer, B. Cornuelle, A. Dzieciuch, W. Munk, P. Worcester, B. Dushaw, B. Howe, J. Mercer, R. Spindel, T. Birdsall, K. Metzger and A. Forbes, "Analysis of multipath acoustic field variability and coherence in the finale of broadband basin-scale transmissions in the North Pacific" *J. Acoust. Soc. Am.* **117**, pp. 1538-1564 (2005)
7. W. Jobst, D. Smith and L. Whited, "Multistatic detection and tracking using linear maximal sequences" *J. Acoust Soc. Am*, manuscript in review, submitted April 2010
8. T. G. Birdsall,, and K. Metzger Jr., "Factor inverse matched filtering" *J. Acoust. Soc Am.* **79**, pp. 91-99 (1986)
9. W. Jobst and L. Dominijanni, "Measurements of the temporal, spatial and frequency coherence of an under water acoustic channel" *J. Acoust. Soc. Am.* **65**, pp. 62-699 (1979)
10. J. Spiesberger, R. Spindel and K. Metzger, "Stability and identification of ocean acoustic multipaths" *J. Acoust. Soc. Am.* **67**, pp. 2011-2017 (1980)
11. H. S. Chang, *Detection of weak, broadband signals under doppler-scaled, multipath propagation* (Ph.D. Dissertation, University of Michigan Dissertation Services 1992), 191 pp
12. H. Deferrari and A. Rogers, "Eliminating clutter by coordinate zeroing" *J. Acoust. Soc. Am* **117**, p. 2494 (2005)
13. P. M. Woodward, *Probability and Information Theory, with Applications to Radar* (McGraw-Hill, New York, 1953),
14. W. Carey, "Lloyd's Mirror- Image Interference Effects", *Acoustics Today*, 5 pp. (2009)